The controllable synthesis, crystal structure and magnetic properties of Mn^{III} Salen-type composite material

Qiong Wu[a,d], Wei Wu[b*], Weili Li[a,d], Yongfeng Qiao[a], Ying Wang[a], Yongmei Wu[c], Baoling Wang[a,d*]

a. Department of Chemical Science and Technology, Kunming University, Yunnan, Kunming 65214, PR China.

b. Department of Physics and Astronomy and London Centre for Nanotechnology, University College london, London, UK.

c. School of International Cultures and Education, Yunnan University of Finance and Economics, Kunming, PR China

d. Yunnan Engineering Technology Research Center for Plastic Films, Kunming University, Kunming, China

** Corresponding authors: ucapwwu@ucl.ac.uk; greenwkm@163.com*

Abstract

By the reaction of manganese-Schiff-base complexes with penta-anionic Anderson heteropolyanion, a new supramolecular architecture $[Mn_2(Salen)_2(H_2O)_2][Mn(Salen)(H_2O)_2]_2Na[IMo_6O_{24}]\cdot 8H_2O$ (**1**) (salen = N,N'-ethylene-bis (salicylideneiminate) has been isolated. Compound **1** was characterized by the single-crystal x-ray diffraction, elemental, IR and thermal gravimetric analyses. Structural analysis reveals that the unit cell simultaneously contains Mn^{III}-Salen dimer and monomer cation fragments, for which the Anderson-type polyanions serve as counter anions. In the packing arrangement, all the Mn^{III} dimers are well separated by polyoxometalate units and form tertiary structure together with Mn^{III} monomers. Interestingly, compared with the previous work, in the exact same reaction conditions, we are able to accurately template Mn^{III}-Salen complexes into different configurations by varying the charge state of polyanions. Besides, the magnetic properties of **1** were also examined by using both dc and ac magnetic field of the superconducting quantum

interference devices. Most importantly, our fitting of the experimental data to a Heisenberg-type spin model showed that there exists a ferromagnetic exchange interaction ~5 K between the spins (S=2) on Mn^{III} in the dimer, while antiferromagnetic ones among monomers and dimer (~ 2 K). In addition, our ac field measurement of the susceptibilities suggested a typical signature for a single-molecule magnet.

Key words**:** Schiff-base, Dimer and Monomer, POM, Single molecule magnet, Magnetic analysis

I. Introduction

Single-molecule magnets (SMM), a type of well-fined nanosized superparamagnetic magnets, have attracted much attention since they were found more than two decades ago [1], not only because of their potential for applications in quantum computing and high-density information storage, but also their flexibility to chemically and structurally manipulate molecular structures, thus making SMM more controllable [2]. In this field, trivalent manganese ions (Mn^{III}) are especially suitable for carrying electron spins owing to their intrinsic large ground state spin quantum number and uniaxial anisotropy [3-5]. Moreover, from the perspective of ligand, the ideal molecular structure should not only be able to stabilize the coordination environment of the metal center, but also have controllable subunits in order to manipulate the reactivity and magnetic behaviors to adapt different synthesis conditions and application environments, respectively. The tetradentate Schiff-base ligands (Salen) and their analogues have been extensively studied and widely used as an important ingredient to elaborate various types of magnetic materials [6-8]. Therefore, in the last a few years Salens have become one of the most booming areas for the construction of molecule-based magnetic materials, especially SMM [9, 10]. So far, a large number of binuclear SMM and single-chain magnets (SCM) compounds based on Mn^{III}-Salen have been isolated. Meanwhile, people have carried out the in-depth study on the structural and magnetic behavior of these compounds, making a series of important scientific progresses and promoting the development of the molecule-based magnetic materials [11-14].

It is worthwhile deepening our study in the synthesis of Salen-type Mn complexes based on the extensive research performed by the other researchers in this field, thus still making the research highly rewarding, such as controllable SMM structures and new effective spin models. Since the Mn-Salen family is an important subunit, a systematic exploration of the relationship between structural and magnetic behaviors can facilitate the rational design and synthesis of molecule-based magnets with new effective spin models [15, 16]. As reported by many researchers, the counter anions of different compositions and structures have a crucial effect on the molecular configuration, spatial arrangement and even magnetic behavior of Mn-Salen complexes [17]. However, since the traditional anions such as NO_3^-, ClO_4^-, Ac^- and other charge pinning are difficult to be further regulated, there is currently little work that has discussed the correlations between the different charge numbers of iso-structural counter anions and the molecular configuration as well as magnetic properties of Mn-salen complexes.

Previously we have used three negative charges in the B-series Anderson-type polyanion $[XMo_6(OH)_6O_{18}]^{3-}$ (X = Al and Cr) to react with classic Mn-Salen complex and successfully isolated Mn-dimer based supramolecular aggregations [18]. Because the molecular configurations of the A and B-series polyanions are exactly the same but their charge states are quite different, they are ideal molecular models to start with. To examine the dependence of structural and magnetic properties on the Coulomb forces, we have selected higher negative charges $[IMo_6O_{24}]^{5-}$ as a precursor to compare with the previous work. Herein, a new monomer-dimer Mn^{III} Schiff-base unit was crystallized in a hybrid compound $[Mn_2(Salen)_2(H_2O)_2][Mn(Salen)(H_2O)_2]_2Na[IMo_6O_{24}]\cdot 8H_2O$ (**1**) and its magnetic properties were studied in details. We have found that (i) our newly synthesized compound was formed by Mn monomer and dimers, (ii) an interesting magnetic interaction structure, i.e., slight spin frustration within the molecular complex, and (iii) most importantly the typical behavior of SMM in this compound.

In the remaining discussion, we first introduce our methods in the section II, discuss our results in the section III, and draw some general conclusions in the section IV.

II. Experimental Details

All related chemicals were purchased and used without further purification. The starting materials $[Mn(salen)(H_2O)]_2(ClO_4)_2 \cdot H_2O$ and $Na_5[IMo_6O_{24}] \cdot 3H_2O$ were synthesized according to the previous work in the literature [19-21] and characterized by infrared (IR) spectroscopy. Elemental analyses for iodide, molybdenum and manganese atoms were analyzed on a PLASMA-SPEC (I) ICP atomic emission spectrometer. The crystallographic data were collected at a temperature of 296(2) K on a Rigaku R-axis Rapid IP diffractometer using graphite monochromatic MoKα radiation (λ = 0.71073 Å). Suitable crystals were mounted in a thin-glass tube and transferred to the goniostat. Multi-scan absorption correction was applied. Iodide, molybdenum and manganese atoms were located by Direct Methods, and successive Fourier syntheses revealed the remaining atoms. Refinements were achieved by the full-matrix method on F^2 using the Shelxtl-97 crystallographic software package [22-24]. In the final refinement, all the non-hydrogen atoms were anisotropically refined. H atoms bonded with the C and N atoms of the Salen ligand were fixed on the calculated atomic positions. The H atoms on the water molecules could not be located from the difference Fourier maps and were directly included in the final molecular formula. The elemental analysis and the charge balance have confirmed their presence. The highest residual peak and the deepest dip are 1.750 and -0.704 e $Å^{-3}$, respectively. The detailed crystal data and structure refinement are given in Table 1. Selected bond lengths and angles are listed in SI (Table S1). Crystallographic data (excluding structure factors) for the structure have been deposited with the Cambridge Crystallographic Data Centre (CCDC), with the depository number CCDC-1057001. IR spectra were recorded in the range of 400 to 4000 cm^{-1} on an Alpha Centaurt Fourier-Transformed IR (FTIR) Spectrophotometer using KBr pellets. Thermal gravimetric (TG) analyses were performed on a Perkin-Elmer TGA-7 instrument in the flowing N_2 with a heating rate of $10°C \cdot min^{-1}$. The

ultraviolet-visible (UV-Vis) absorption spectrum was obtained using a 752 PC UV-Vis spectrophotometer. The magnetic susceptibility measurements were carried out with the use of a Superconducting Quantum Interference Device (SQUID), produced by Quantum Design, magnetometer MPMS-XL. The magnetic measurements were performed on a polycrystalline sample of 18.83 mg, which has been examined by FTIR and UV-Vis spectroscopies. The AC susceptibility of the same sample has been measured with an oscillating ac field with an amplitude of 500 Oe and the frequencies ranging from 100 to 1200 Hz. The diamagnetic corrections for the compound were estimated using Pascal's constants, and magnetic data were corrected for diamagnetic contributions of the sample holder as well [25].

Synthesis

$Na_5[IMo_6O_{24}]\cdot 3H_2O$ (1.26 g, 1.0 mmol) was dissolved in 20 ml distilled water. Then, 20 ml methanol solution containing freshly prepared $[Mn(salen)(H_2O)]_2(ClO_4)_2\cdot H_2O$ (0.88 g, 1 mmol) was quickly added to above solution. The dark-brown reaction mixture was sealed and stirred in a conical flask at 35 °C for 2 days. After filtration, the filtrate was slowly evaporated at room temperature. After filtration, the filtrate was sealed with parafilm containing tiny pores for facilitating slow evaporation at room temperature. Dark-brown stick-like crystals of compound **1** were isolated after one week. After filtration, the remaining 31% were washed with methanol and dried in the air. The chemical formula for the compound **1** is $C_{34}H_{56}Mn_2N_7IMo_6O_{45}$. We found the percentages of the elements, compared with the theoretical values, are as follows: 19.11 (19.49) % for C, 5.16 (4.68) % for N, 5.26 (5.98) % for I, 5.76 (6.05) % for Mn, 29.12 (27.36) % for Mo. TG analyses have indicated that there are approximately 6 lattice water molecules in the unit cell of the compound (See SI-Fig. S3).

III. Results and Discussion

Materials Synthesis

In order to study the effect of different charge counterions on the structure and magnetic properties of Mn-salen compounds, in this work, we have selected B-series Anderson-type polyanion $[IMo_6O_{24}]^{5-}$ as a research object and compared its structure and properties with the previous results [18]. In order to rule out the effects of other factors, we have used the same synthetic scheme as reported before. The reaction phenomena and crystallization times in the synthesis process are basically the same as before.

Crystal Structure

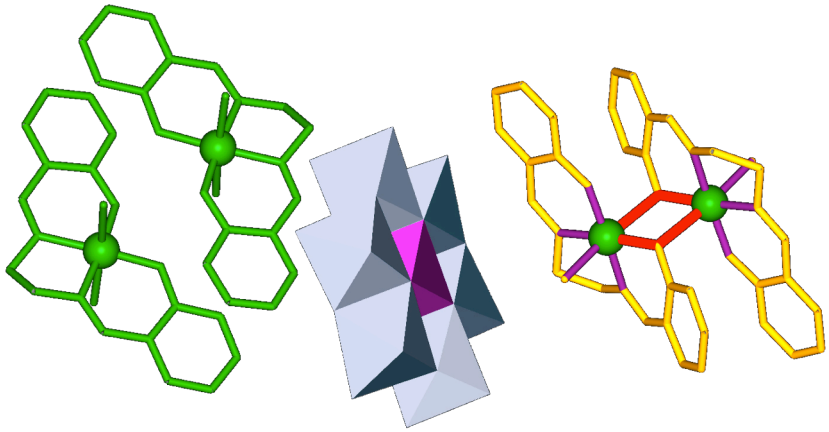

Fig. 1: The supramolecular architecture of $[Mn_2(Salen)_2(H_2O)_2][Mn(Salen)(H_2O)_2]_2Na[IMo_6O_{24}]\cdot 8H_2O$ (**1**), by combining polyhedral and ball-and-stick molecular representations. In $[IMo_6O_{24}]^{5-}$ (middle), Mo is represented by gray octahedral and I by purple octahedral. In $[Mn(Salen)(H_2O)]_2^{+}$ (right): Mn is represented by green ball; C, N, and O atoms by yellow balls. Mn-O_{Ph} bonds are represented by red sticks. $[Mn(Salen)(H_2O)_2]^{+}$ monomers are represented by green balls and sticks.

Single-crystal x-ray diffraction structural analysis reveals that the compound **1** crystallizes in the triclinic space group *P-1*, and is constructed from an A-type heteropolyanion, $[IMo_6O_{24}]^{5-}$, an out-of-plane $[Mn(Salen)(H_2O)]_2^{+}$ dimeric moiety, and two $[Mn(Salen)(H_2O)_2]^{+}$ monomers. As illustrated in Fig. 1 and S1, there is a half of typical A-type polyanion $[IMo_6O_{24}]^{5-}$ structure motif in

the asymmetric unit of the compound **1**, in which heteroatoms are situated in specific positions with 50% occupancy rate. The $[IMo_6O_{24}]^{5-}$ segment is composed of seven edge-sharing $\{XO_6\}$ octahedra, one of which is located at the center of polyanion and surrounded by six $\{MoO_6\}$ octahedra. In addition, according to the oxygen-coordination environments, Mo-O bonds can be classified into three types: terminal oxygen O_t (1.694(4)-1.712(6) Å), double-bridging oxygen O_b (1.898(5) - 1.933(5) Å), central oxygen O_c (1.883(5)-2.357(5) Å).

In dimeric $[Mn_2(Salen)_2(H_2O)_2]^{2+}$ unit (*abbr.* $[Mn_2]$), the Mn^{III} ions are coordinated by six oxygen atoms in an octahedral geometry, whose equatorial plane is occupied by N_2O_2 atoms from the $Salen^{2-}$ ligand, with average bond legnths: d (Mn-O) = 1.890 Å and d (Mn-N) = 1.953 Å. The axial positions are occupied by a water molecule and a phenoxy oxygen ($O_{Ph'}$) atom from the other halve of salen ligand, resulting in an overall centrosymmetric dimeric structure as shown in Fig. 2. These coordination modes and bond lengths are close to the salen-type manganese dimer complexes reported previously [18].

Different from the previous work, there are two monomeric units crystallized $[Mn(Salen)(H_2O)_2]^{+}$ (abbr. $[Mn_1]$) in the supramolecular architecture. Mn^{III} ions in monomers also possess a distorted octahedral geometry, in which the equatorial plane is defined by two N_2O_2 from the salen ligand. Nevertheless, different from $[Mn_2]$ moiety at the apical site, the Mn^{III} center is coordinated with two water molecules; the related bond lengths are 2.270(5) Å (O_1W-Mn_2) and 2.275(5) Å (O_1W-Mn_2), receptively. It is worth noting that a cocrystallized configuration, including Mn-Schiff-base complexes, monomer and dimer, is rarely observed [26]. After performing the structural analysis by using PLATON software [27], we found that two monomers are linked to each other via O-H...O hydrogen bonds between apical water molecule (O_{18}) and adjacent phenoxy

oxygen (O_{13}) atoms, while the π-π stacking interactions between adjacent benzene ring are responsible to form a self-assembled supramolecular dimer. Interestingly, similarly linking mode occurs between adjacent [Mn_1] and [Mn_2] units. The O-H...O hydrogen bonds connect [Mn_2] and [Mn_1] fragments to generate one-dimensional '[Mn_1]-[Mn_2]' supramolecular chains along the crystallographic *b*-axis (See Fig. 2(a)). The details for the hydrogen bonds are listed in Table.2. Owing to the co-crystallization of polyoxometalates (POMs) and [Mn_1] units, the [Mn_2] dimers are well dispersed between POMs and [Mn_1], thus forming a tertiary structure. The shortest distance between [Mn_2] dimer through POMs units and [Mn_1] unit is 13.59 Å and 14.45 Å, respectively (See Fig. 2(b)). Such a distance is sufficiently long to eliminate the intermolecular magnetic interaction and thus retain the intrinsic single-molecular magnetic properties of the compound **1**.

Table 1: Crystal data and structure refinements for **1**

Compound	**1**
Empirical formula	$C_{64}H_{68}IMn_4Mo_6N_8NaO_{44}$
Formula weight	2649.1(9)
Temperature (K)	293(2) K
Wavelength, (Å)	0.71073 Å
Crystal system	triclinic
Space group	$P\bar{1}$
a(Å)	14.204(3)
b(Å)	14.876(3)
c (Å)	14.877(3)
$\alpha(^o)$	92.33(3)
$\beta(^o)$	111.67(3)
$\gamma(^o)$	112.03(3)
Volume ($Å^3$)	2649.1(9)
Z	1
Calculated density (g cm^{-3})	1.629
Absorption coefficient (mm^{-1})	1.521
F(000), e	2628

θ range for data collection	3.01 - 25.00°
Limiting indices	-16≤h≤16, -17≤k≤17, -17≤l≤17
Reflections collected / unique / R_{int}	20696 / 9268/ [R(int) = 0.0310]
Completeness to theta = 25.00, %	99.20%
Refinement method	Semi-empirical from equivalents
Data / restraints / parameters	9268 / 5 / 613
Goodness-of-fit on F^2	1.064
Final R indices [I > 2σ(I)]	R1 = 0.0509, wR2 = 0.1230
R indices (all data)	R1 = 0.0649, wR2 = 0.1274
Largest diff. peak and hole	1.750 and -1.51 e.Å^{-3}

$^{a}R_1 = \sum||F_0|-|F_C||/\sum|F_0|$; $^{b}wR_2 = \sum[w(F_0^2-F_C^2)^2]/\sum[w(F_0^2)^2]^{1/2}$

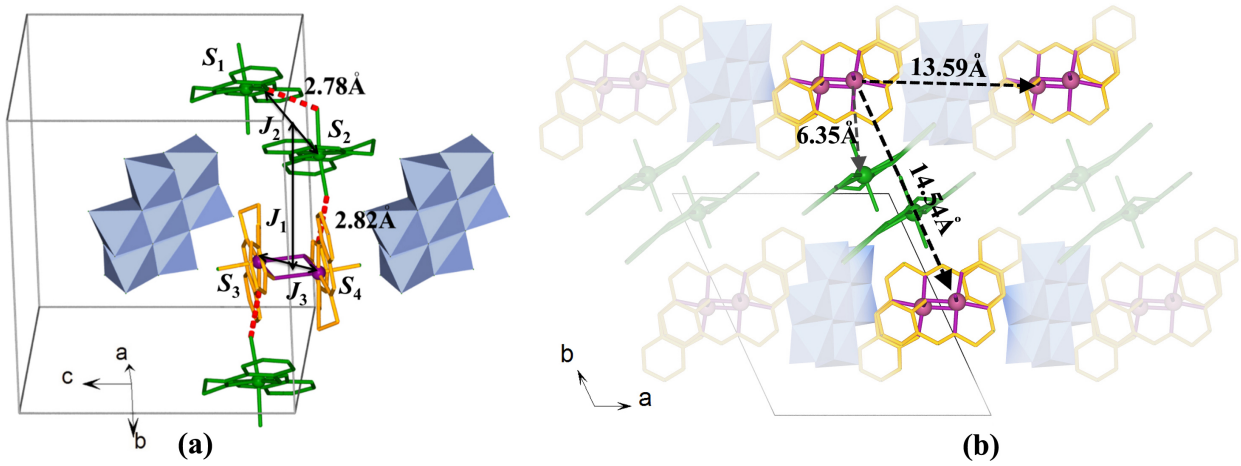

Fig. 2: The packing arrangement of compound **1** on the [001] plane (a) and along (001) direction (b), exhibiting the nearest intra and intermolecular Mn...Mn distance in **1**. Lattice water molecules are omitted for clarity. In (a), we defined the related exchange interactions between Mn^{III} ions (S=2) in the diagram. J_1 is the exchange interaction between monomers (S_1 and S_2) and dimer (S_3 and S_4), J_2 between S_1 and S_2, and J_3 between S_3 and S_4.

Table 2: Hydrogen-bond parameters (Å for distances; ^{o} for angles) for **1**

D-H···A	D-H	H···A	D···A	D-H···A
O(18)-H(18C)···O(13)	0.79(8)	2.28(9)	2.820(7)	127(7)
O(19)-H(19B)···O(14)	0.86(6)	1.98(6)	2.778(6)	155(8)
O(19)-H(19C)···O(16)	0.81(6)	2.09(6)	2.727(7)	136(6)

Magnetic measurements

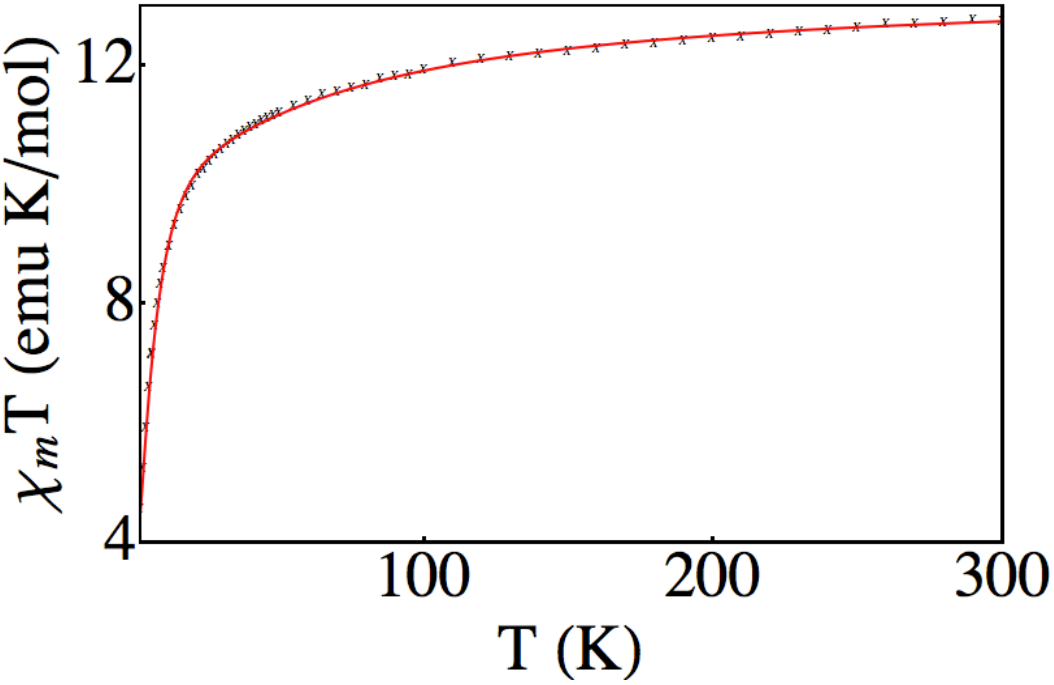

Fig. 3: Temperature dependence of the $\chi_m T$ for **1**. The crosses are experimental results for $\chi_m T$. The solid red curve is the fitting based on the Hamiltonian and exchange interactions defined in the text, which is in an excellent agreement with the experiment. The fitted values for J_1, J_2, J_3 and g-factor are -2.00, -2.54, 5.33 K, 2.1057, respectively.

Although the variety of the structures of the Mn-salen family of compounds has been very rich, the vast majority of the structures of the Mn-salen fragments isolated from the compounds is formed by a single type of configuration. However, now we have a combination of compounds of various configurations, which is rare. The spin-2 on Mn^{III} originates from the octahedral crystal-field environment of the Mn^{III}, and the fact that the on-site Coulomb interaction for d-orbital is much larger than the crystal-field splitting, thus forming a high-spin state. For its magnetic properties, we

have used a simple magnetic model to perform an in-depth analysis to understand the nature of the exchange interactions between Mn^{III} spins. The temperature dependence of the magnetic susceptibility has been studied in the range of 2 to 300 K. The measured $\chi_m T$ versus T plot of **1** is shown in Fig. 3. The susceptibility data were fitted by a Heisenberg-type spin Hamiltonian that reads $\hat{H} = -2J_1(S_1 + S_2)\cdot(S_3 + S_4) - 2J_2 S_1 \cdot S_2 - 2J_3 S_3 \cdot S_4 - g\mu_B B_z(S_{1z} + S_{2z} + S_{3z} + S_{4z})$, where J_1 can be understood as an averaged exchange interaction between the Mn monomers and the Mn dimer, J_2 is the exchange interaction between monomes, and J_3 between Mn^{III} within the dimer. Since the A-type polyanion and $[IMo_6O_{24}]^{5-}$ units in **1** are expected to be diamagnetic, therefore, the magnetic properties of **1** should originate from the interactions between the spins on Mn^{III} ions [28]. Notice that here we neglected the spin anisotropy because based on the $\chi_m T$ measurements the anti-ferromagnetic interactions among the spins seem more important. When the temperature was lowered, the $\chi_m T$ values at room temperature is measured to be approximately 12.10 $cm^3mol^{-1}K$, which is close to the high-temperature limit for a total spin of 4 Mn^{III} ions (S = 2, g = 2). When the temperature was lowered, the $\chi_m T$ value decreases steadily and reaches a minimum value of 4.73 $cm^3mol^{-1}K$ at 6.2 K, indicating the presence of antiferromagnetic interactions among Mn^{III} centers. However, **1** contains two types of Mn-salen fragments. We have then fitted the experimental date by the above Heisenberg Hamiltonian, and found the best fitting parameters for J_1, J_2, J_3 and g-factor are -2.00, -2.54, 5.33 K, 2.1057, respectively. The fitted value for J_3 (ferromagnetic) is in qualitative agreement with that reported previously [29]; the discrepancy might be owing to the omission of zero-field splitting [30]; otherwise the compound synthesized here is slightly different from that in Ref. [29]. However, this ferromagnetic interaction is the most dominant term in the Hamiltonian apart from the region with high magnetic field. The origin of the ferromagnetic interaction might be the indirect exchange owing to the bridging O atoms between the Mn^{III} ions within the dimer [31]. The other two interactions are anti-ferromagnetic, which is consistent with the experimental curves. This anti-ferromagnetic interaction can be understood as the super-exchange interaction between two high-spin states between stacked molecules [32]. Note that there is a slight frustration (as illustrated in Fig.5) that may occur at very low temperature (kT < Min[J_1, J_2]) as J_1 and J_2 are both anti-ferromagnetic because in this temperature range the Mn dimer can be approximately seen as a single magnet. This might be one of the most important driving forces for the SMM behavior [33].

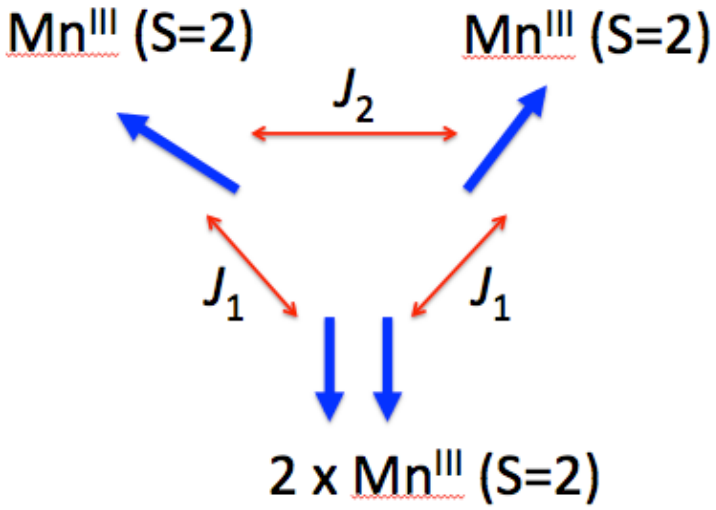

Fig.4: An illustration for the spin frustration among spins in compound **1**.

The slow relaxation behavior of the magnetization of **1** has been studied using AC susceptibility measurements with a series of ac magnetic fields with a magnitude of 5 Oe, as a function of frequencies (100-1200Hz) and temperatures (2-6.5 K). As shown in Fig.6 (a) and (b), No maximum was observed, but the frequency-dependent χ'' shows the signals below 5 K, indicating the slow magnetization relaxation, a typical behavior for SMM. At zero DC field, a frequency-dependent out-of-phase ac signal is detected between 2 and 6 K. Unfortunately the relaxation time cannot be determined from the χ'' as even at 2 K the peaks have appeared.

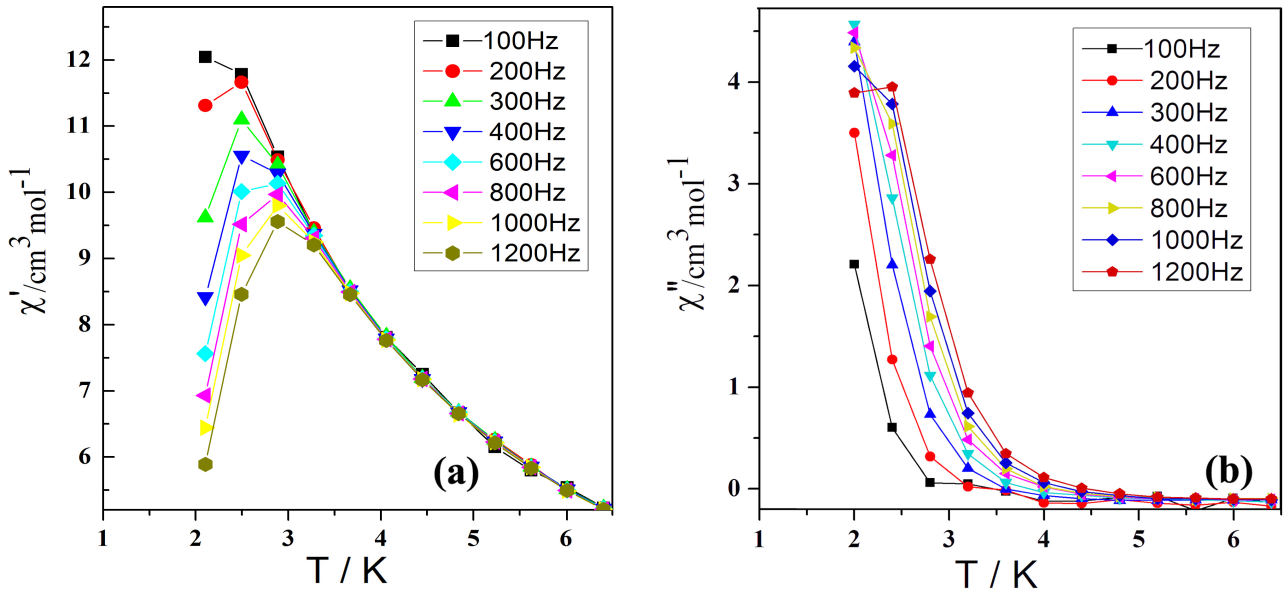

IV. Conclusions

By using the counterions with different molecular configurations having the same charge state, we have isolated a new type of Mn-Salen complex with the coexistence of the monomer and dimer structures. This work demonstrated the effect of the amount of charge (equivalently the different size of the Coulomb forces) on the coordination of the metal complex during the crystallization process. This methodology could be important for the further design and construction of molecule-based magnetic materials. Our SQUID DC magnetic measurements showed that there exist both strong anti-ferromagnetic (between monomer and dimer) and ferromagnetic interaction (within the dimer), which is much larger than the spin anisotropy reported previously. The combination of both types of exchange interactions suggests that a meta-magnetic state should be present in this complex. Our AC magnetic measurements, including the real and imagninary parts, indicated that the compound consists of SMM, which would have great potential in my applications. In the future, we would like to introduce other POM precursors to act as inorganic building blocks, bridges, or spacers for new types of supramolecular architectures.

Acknowledgement. This work was supported by Fund for Less Developed Regions of the National Natural Science Foundation of China (No.31760257); National Natural Science Foundation of China (No.21201090); Agricultural plastic film and products research and development of Plateau area (No·DH1606).

Supporting information

Detailed bond lengths and angles, packing arrangement, IR spectra as well as TG analysis are given as Supporting Information (SI) available online.

Reference

[1] R. Sessoli, H.L. Tsai, A.R. Schake, S. Wang, J.B. Vincent, K. Folting, D. Gatteschi, G. Christou, D.N. Hendrickson, J. Am. Chem. Soc., **115**, 1804 (1993).

[2] W. Wernsdorfer, N. Aliaga-Alcalde, D.N. Hendrickson, G. Christou, Nature, **416** 406 (2002).

[3] C. Ritchie, A. Ferguson, H. Nojiri, H.N. Miras, Y.-F. Song, D.-L. Long, E. Burkholder, M. Murrie, P. K'gerler, E.K. Brechin, L. Cronin, Angew. Chem. Int. Ed., **47**, 5609 (2008).

[4] Y.-W. Li, Y.-G. Li, Y.-H. Wang, X.-J. Feng, Y. Lu, E.-B. Wang, Inorg. Chem., 48 (2009) 6452-6458.

[5] X. Fang, P. Kögerler, Y. Furukawa, M. Speldrich, M. Luban, Angew. Chem. Int. Ed., **50**, 5212 (2011).

[6] Y.B. Shu, W.S. Liu, Dalton Trans, **44**, 6353 (2015).

[7] J. Li, J. Yang, Y.Y. Liu, J.F. Ma, Chemistry - A European Journal, (2015).

[8] X. Yang, R.A. Jones, S. Huang, Coordination Chem. Rev., **273**, 63 (2014).

[9] Q. Wu, Q. Pu, Y. Wu, H. Shi, Y. He, J. Li, Q. Fan, J. Coord. Chem., **68**, 1010 (2015).

[10] H. Miyasaka, A. Saitoh, S. Abe, Coord. Chem. Rev., **251**, 2622 (2007).

[11] T. T. Wang, M. Ren, S. S. Bao, Z. S. Cai, B. Liu, Z. H. Zheng, Z. L. Xu, L. M. Zheng, Dalton Trans, **44**, 4271 (2015).

[12] P. Seth, S. Ghosh, A. Figuerola, A. Ghosh, Dalton Trans, **43**, 990 (2014).

[13] Y. Sawada, W. Kosaka, Y. Hayashi, H. Miyasaka, Inorg. Chem., **51**, 4824 (2012).

[14] T. Glaser, Chem. Commun., **47**, 116 (2011).

[15] T.-T. Wang, S.-S. Bao, M. Ren, Z.-S. Cai, Z.-H. Zheng, Z.-L. Xu, L.-M. Zheng, Chemistry – An Asian Journal, **8**, 1772 (2013).

[16] Q. Wu, H. Liu, X. Hu, J. Lu, H. Wang, J. Clust. Sci., **26**, 1203 (2015).

[17] C. Kachi-Terajima, R. Ishii, Y. Tojo, M. Fukuda, Y. Kitagawa, M. Asaoka, H. Miyasaka, J. Phys. Chem. C, **121,** 12454 (2017).

[18] Q. Wu, Y.-G. Li, Y.-H. Wang, R. Clérac, Y. Lu, E.-B. Wang, Chem. Commun., 5743 (2009).

[19] H. Miyasaka, R. Clerac, T. Ishii, H.-C. Chang, S. Kitagawa, M. Yamashita, Dalton Trans., 1528 (2002).

[20] G.T. Musie, X. Li, D.R. Powell, Inorganica Chimica Acta, **357**, 1134 (2004).

[21] M. Filowitz, R.K.C. Ho, W.G. Klemperer, W. Shum, Inorg. Chem., **18**，93 (1979).
[22] G.M. Sheldrick, Acta Crystallogr, A **64**，112 (2008).
[23] G.M. Sheldrick, Bruker Analytical X-ray Instruments Inc., Madison, WI (USA) (2001).
[24] G.M. Sheldrick, SHELXL-97, Program for Solution of Crystal Structures, University of Göttingen, Germany, (1997).
[25] E.A.L. Boudreaux, L.N. Mulay, Book Review: *Theory and applications of molecular paramagnetism*. Edited by E. A. Boudreaux and L. N. Mulay. Wiley-Interscience, New York, 1976.
[26] M. Okuhata, T. Mochida, Polyhedron, **43**, 153(2012).
[27] A.L. Spek, Acta Crystallogr, D**65**, 148 (2009).
[28] C.P. Landee, M.M. Turnbull, J. Coord. Chem,, **45**, 375 (2014) .
[29] L. Lecren, W. Wernsdorfer, Y. Li, A. Vindigni, H. Miyasaka, and R. Clrac, J. Am. Chem. Soc., **129** (16), 5045 (2007).
[30] B.J. Kennedy, K.S. Murray, Inorg Chem,, **24**, 1552 (2002) .
[31] Wei Wu, A. Kerridge, A. H. Harker and A. J. Fisher, Phys. Rev. B **77**, 184403 (2008).
[32] Wei Wu, A. J. Fisher, and N. M. Harrison, Phys. Rev. B **88**, 224417 (2013).
[33] O. Cador, D. Gatteschi, R. Sessoli, A. Barra, G. A. Timco and R. E. P. Winpenny, J. Magn. Magn. Mater, **290**, 55 (2005).